3D Multi-pass finite element welding modelling of butt-welded plate specimen

Sanz Balduz, Luis Javier[1]; Salesa Bordanaba, Ángel[2]; González Abril, Emilio[3]

ABSTRACT

A multi-pass welding of a thin rectangular (dog-bone shaped) butt joint plate is numerically simulated as a coupled thermo-mechanical transient problem. The simulation uses an "element-birth" technique to simplify the complexity of the problem. The paper discusses the challenges of the simulation of a multi-pass weld problem and the utility of the results for practical applications.

The final solution shows crucial stress distributions in a challenging geometry where large thermal transients and gradients are created by the welding procedure. The results also indicate the plastic yielding of the weld-joint after extensive cooling of the joined plate. The displacements from the results can be used to estimate the extent of distortions qualitatively. Despite minimal resources (2 CPUs on a standard Intel desktop architecture and 2 GB RAM over duration of 4 days) the procedure is able to provide adequate details in predicting residual stresses for multi-pass welded components.

Keywords: Steel, welding, finite elements, element-birth, multi-pass

1. INTRODUCTION

The butt joint weld between two St-52.3N steel plates is simulated. The joint is created finally from three welding passes, first of them with TIG and the last with GMAW (Fig. 1). The successive welding passes add material to the joint between two plates separated by a fixed distance. In order to accommodate sufficient filler material, the plate edges are bevelled creating a chamfer of 60 degrees between them [1].

The simulation assumes a surface welding flux of Gaussian distribution. The molten weld-material is added in successive stages as the weld-torch moves along the weld joint using the birthing process. The activated elements in the weld pool are at a higher temperature of the material and act as a heat source in addition to the surface flux from the weld-arc. The discrete addition of the weld material to the simulation geometry approximates the rate of addition of weld material. As the torch moves away from the newly added material, the overall temperature of the weld pool decreases on account of phase change causing fusion between the weld pool and the heat-affected zone (HAZ). The two plates in the joining process have mechanical restraints that lead to the peculiar residual stresses and

[1] Imagina, SLP (SPAIN). ljsanz@imgn.net (Corresponding author)
[2] Imagina, SLP (SPAIN). asalesa@imgn.net
[3] Indipes, SLP (SPAIN). egabril@ciccp.es

3D Multi-pass finite element welding modeling of butt-welded plate specimen
Third International Conference on Mechanical Models in Structural Engineering
University of Seville. 24-26 june 2015.

distortions produced during this fusion process. Successive welding passes are performed after a cooling period to allow the temperature distribution in the plates to fall sufficiently.
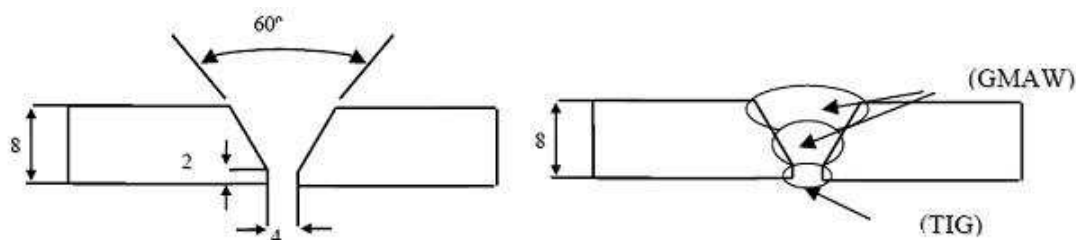

Figure 1. *Schematic for plate specimen for butt welding.*

2. MODEL DESCRIPTION

2.1. Specimen Geometry and Material Properties

2.1.1. Geometry

A standard ASTM tensile test specimen, cut halfway along the length, is used for butt-weld analysis. This geometry (Fig. 2) is conveniently chosen as once the two halves are joined as a butt-weld, it is subsequently tested for tensile strength. Initially a specimen with thickness of 20 mm was chosen for the purpose of modelling and simulation. However, this geometry required 6 weld passes to finish the butt-weld. Considering the computational cost involved in the simulation of the 6 passes an alternate geometry with 8 mm thickness was chosen for this study. With this sample, the smaller thickness does provide higher temperature gradients across thickness causing higher distortions for the same heat input and subsequent computational demands. However, the butt-weld joint requires only three weld passes to finish reducing overall computational effort required for simulation. Table 1 shows the relative volumes of the filler material deposited during each pass.
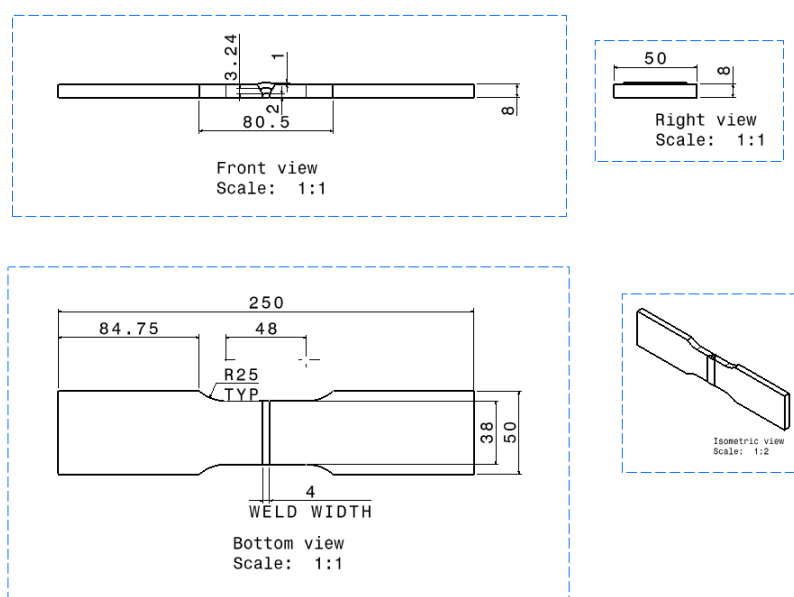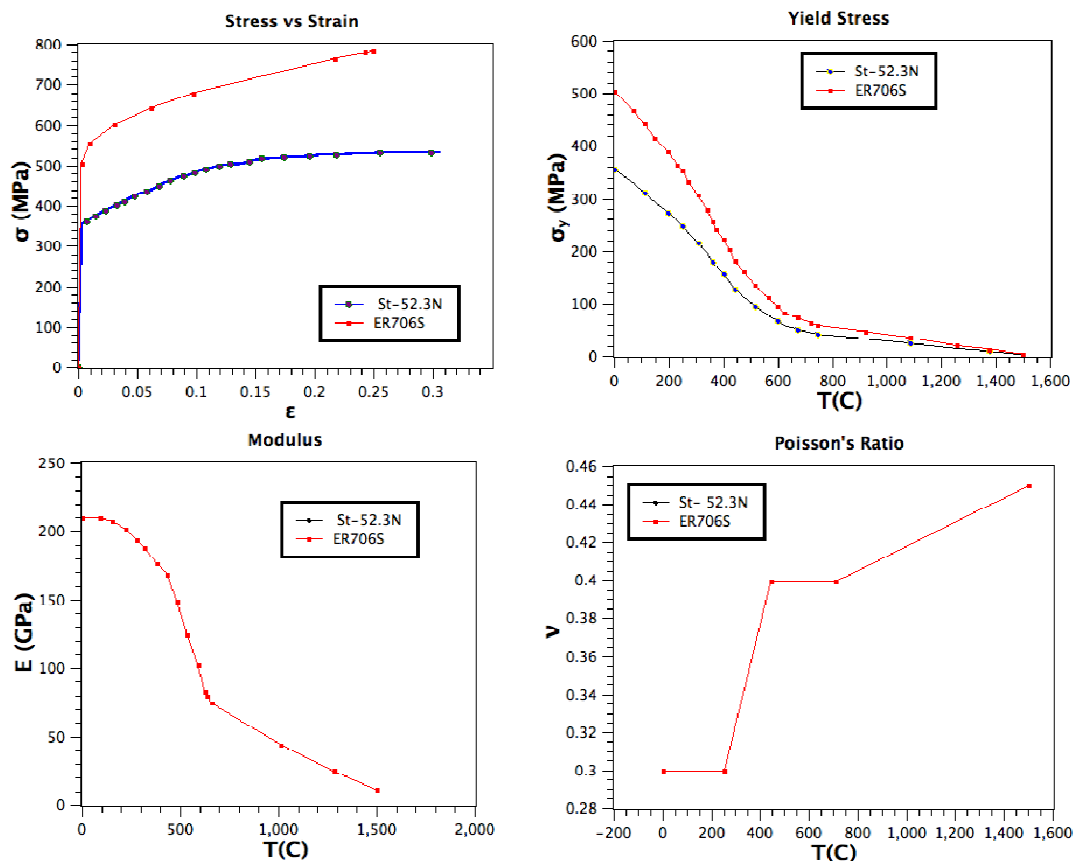

Figure 2. *Schematic of plate used in modelling butt-weld (mm).*

Luis Javier Sanz Balduz[1], Ángel Salesa Bordanaba[2] and Emilio González Abril[3]

Table 1. Pass-wise volumes for filler material

Weld Pass	Volume (mm^3)	Volume-ratio
Pass 1	379	1
Pass 2	738.8	1.95
Pass 3	1164.5	3.07

2.1.2. Material Properties

The filler weld material deposited as part of the arc welding process (TIG/GMAW) has different material properties than the material for the plates involved in the butt-welding process. In the current study, the plate material used is a steel (ST-52.3N; ISO FE-510 D) with a high carbon filler weld material (ER706S). Considering the large temperature range involved in the joining process, the model needs to address the changes in the mechanical and thermal properties over the given range. The mechanical and thermal properties for the plate and weld materials are shown in Figure 3 and 4 respectively.

Figure 3. *Structural properties for ST-52.3N and ER706S.*

9

3D Multi-pass finite element welding modeling of butt-welded plate specimen
Third International Conference on Mechanical Models in Structural Engineering
University of Seville. 24-26 june 2015.

The filler material (ER706S) maintains thermal properties nearly identical to those of the ST-52.3N. Yet, there is a slight modification in its structural properties.
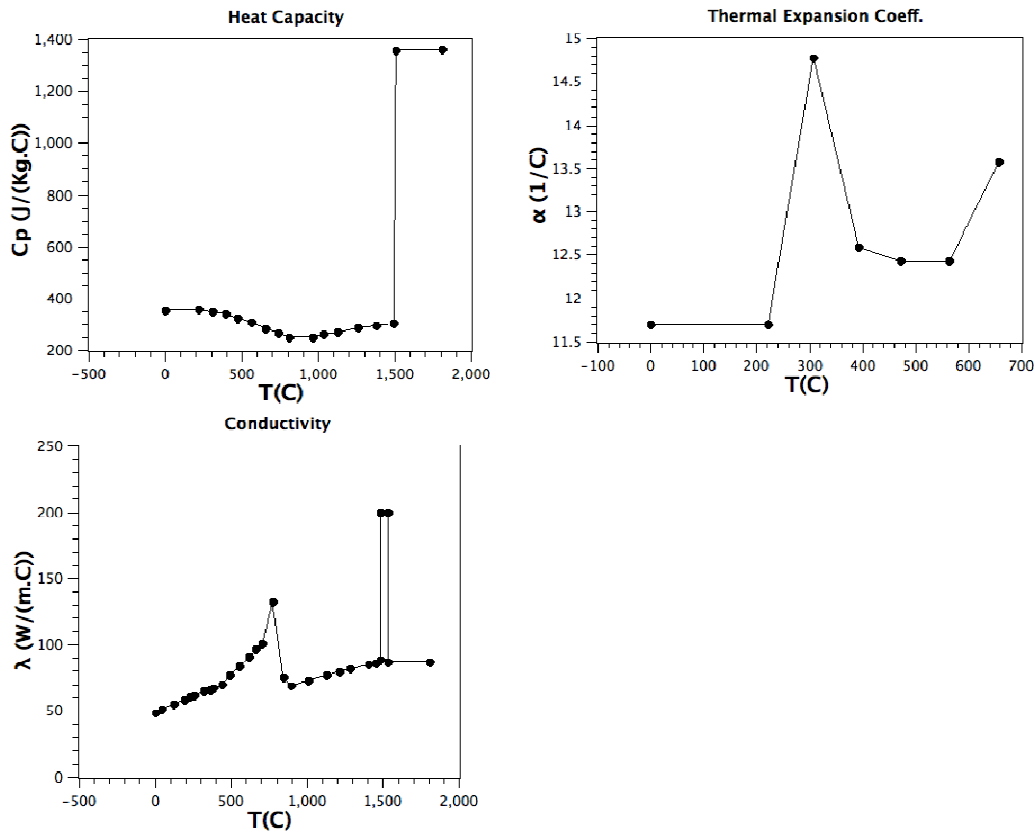

Figure 4. *Thermal properties for ST-52.3N and ER706S.*

2.1.3. Material Model Implementation in ABAQUS

During the welding process, the weld pool and the heat affected zone undergo significant temperature changes with the exposure of the welding-arc. The modulus and the yield stress changes over this temperature, residual stresses at the end of the procedure are a function of these temperature changes and the restraints on the welding plate. The code used for simulation (ABAQUS 6.9) allows specification of the material properties (Young's modulus and yield stress) through the *ELASTIC and *PLASTIC commands. Based on the available experimental data for elastic modulus and yield stress as function of the temperature, isochronous plasticity curves are extrapolated. This is a reasonable assumption as the data for stress-strain experiments at various temperatures and strain rates are not available. This procedure allows creep behaviour description from thermal changes, which tend to dominate during the welding process. In addition materials under high loads tend to show significant creep stress under high strain rate conditions. Currently, the rate dependence of material properties is not modelled to simplify the scheme.

2.2. Welding Procedure

The welding process discussed here produces a high voltage arc between the metal electrode and the work-piece. The arc is shrouded with an inert gas that shields the environment around the arc and the weld pool to reduce oxidation or other chemical reactions from exposure to the environment (Fig. 5). The arc welding process used for joining the plates for the first pass is a Tungsten Inert Gas welding (GTA or TIG) process where as the subsequent passes use the Metal Inert Gas (MIG or GMAW) method.
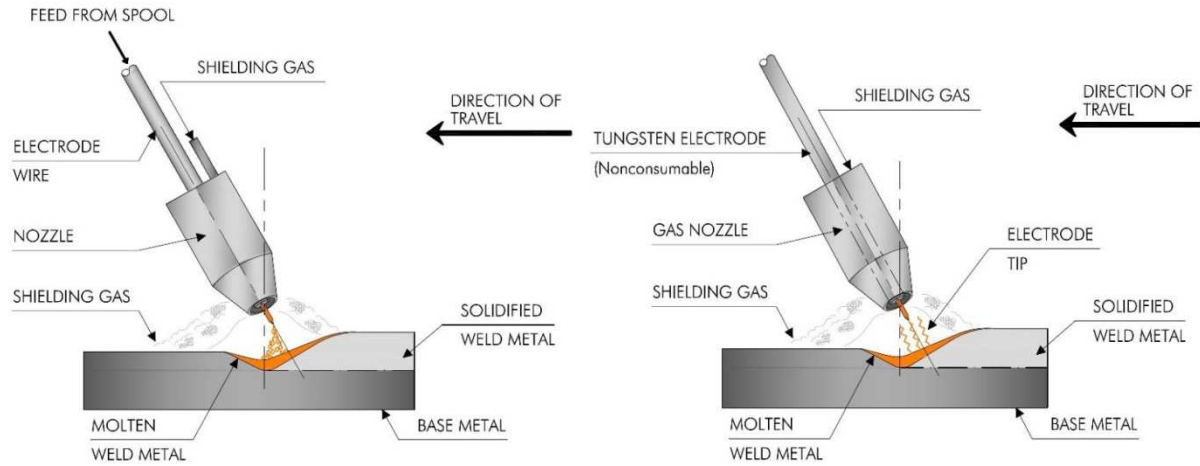

Figure 5. *Illustration of arc welding processes: GMAW (left) and TIG welding (right) [1].*

The TIG process differs from GMAW in its usage of non-consumable electrode. This process may involve a filler material rod or in some cases joining of materials by fusion. On the other hand the GMAW process uses a consumable electrode made of filler material. The TIG process may require higher levels of skill and less tolerant to automation. The GMAW process is easy to automate. At the same time, the TIG process is applicable to a range of metals where as the GMAW has relatively limited applicability across materials. Table 2 shows the DC voltage and current settings assumed for the current model.

Table 2. Power setting and torch speed for the butt welding passes

Pass	Weld	Current	Voltage	V·I	Travel Speed (cm/min)	Efficiency	Heat Input (kJ/cm)	Volume Ratio to 1st pass
1	TIG	100 A	14 V	1400	12	0.60	4.20	1.00
2	GMAW	105 A	19 V	1995	6.0	0.80	7.98	1.95
3	GMAW	120 A	19 V	2280	4.0	0.80	9.12	3.05

2.3. Computational Model Implementation

The finite element model for the butt-weld joint is created in ABAQUS 6.9 (Dassault Systems) environment. The procedure implemented for this problem uses a fully-coupled thermo-mechanical

3D Multi-pass finite element welding modeling of butt-welded plate specimen
Third International Conference on Mechanical Models in Structural Engineering
University of Seville. 24-26 june 2015.

system of equations over the discretized geometry of the finite element mesh. The coupled thermo-mechanical system then solves the heat-balance equation and the momentum-balance equation.

ABAQUS uses a nonlinear Newton-Raphson procedure with second order convergence rate for minimizing the residuals for the entire set of equations (temperatures and displacements). The resulting assembled stiffness matrix is highly unsymmetrical (especially for temperature dependent thermal properties). Also the thermal expansion from change in temperature affects the momentum balance through the displacement term where-as the dissipative effects such as heat generated from large inelastic deformations affect the temperature distribution. In the current problem, the material in the weld-pool is heated above the melting point causing phase change. There is also a second phase change from liquid to solid as the weld-pool cools down at the end of a pass. These phase changes are accounted through internal energy changes in the thermal equation.

2.3.1. Mesh Discretization and Element Birth Technique

Figure 6 shows the mesh used for the butt-weld model with colour coded element sets to indicate the heat affected zone and weld pool with three distinct passes. The coupled reduced integration 8 noded elements (C3D8RT) have first order temperature and displacement interpolation functions. These are generally robust and computationally efficient for large deformation non-linear problems.
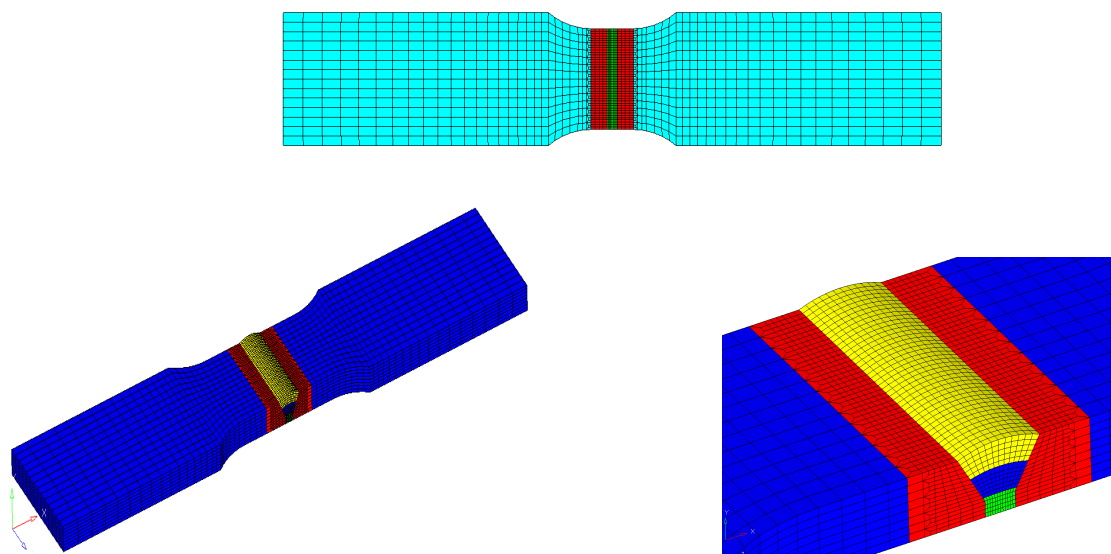

Figure 6. *Mesh used. HAZ (red) and welding passes (Pass1: Green; Pass2: Dark blue; Pass3: Yellow)*

The primary source of heat in the current problem is from the weld-arc travelling along the joint. The heat from the arc melts the filler material through volumetric heating. Additionally the weld-arc also provides surface heating to the deposited filler material in weld-pool as well as the work-piece area under its influence (HAZ). This secondary heating is essential mechanism in fusing the filler material to the work-piece. To simplify the computational procedure, the actual melting of filler material from the

weld arc is not considered as part of the simulation. Instead, elements in the weld-pool are activated to coincide the passage of the weld-arc. This rate of element activation is set to match the filler deposition rate effectively reducing computational complexity behind the filler melting procedure. Based on experimental data for the procedure, an activation temperature of 2000°C was initially assigned for the newly activated material. Also based on several iterations with the model to ascertain the requirement for discretization and a smooth solution, the weld-arc path was divided into small time steps. Once the coupled-temperature displacement solution procedure is used to solve the equation for the duration of the step, a new set of elements are activated. The process used in simulating the birthing mechanism is illustrated in Figure 7. Once the weld-travel along the weld-line is complete for a given pass, a cooling period is simulated before the next pass. The ABAQUS implementation of element birthing process uses the *MODEL CHANGE command option to emulate the birthing process for the elements in the weld pool. At the beginning of a weld-pass all the weld-pool elements are deactivated using this command. As the weld-arc travels along the weld-line, a set of elements is activated (birthed) to represent the addition of the filler material. Since the birthed elements represent filler material in liquid state, the elements are assumed strain free when activated in this manner. Once the weld-arc travels to the end of the newly added elements, a subsequent ABAQUS step adds (births) a new set of elements to the active geometry. At any given time increment, the calculation of stress and temperature field solution is illustrated by the algorithm shown in Figure 8. The weld-pass is finished once all the elements in the weld-pool activated and the weld-torch moves from one end of the weld-piece to the other end. Before additional filler material is added through another pass, typically the weld-pieces are allowed to cool so that the weld-pool fusion with the weld-pieces is sufficiently solidified and the weld-joint has reached a relatively steady state stress-field. The length of the cooling period after each pass was determined based on the minimum time required for the weld-piece to reach temperatures to 250°C or less.
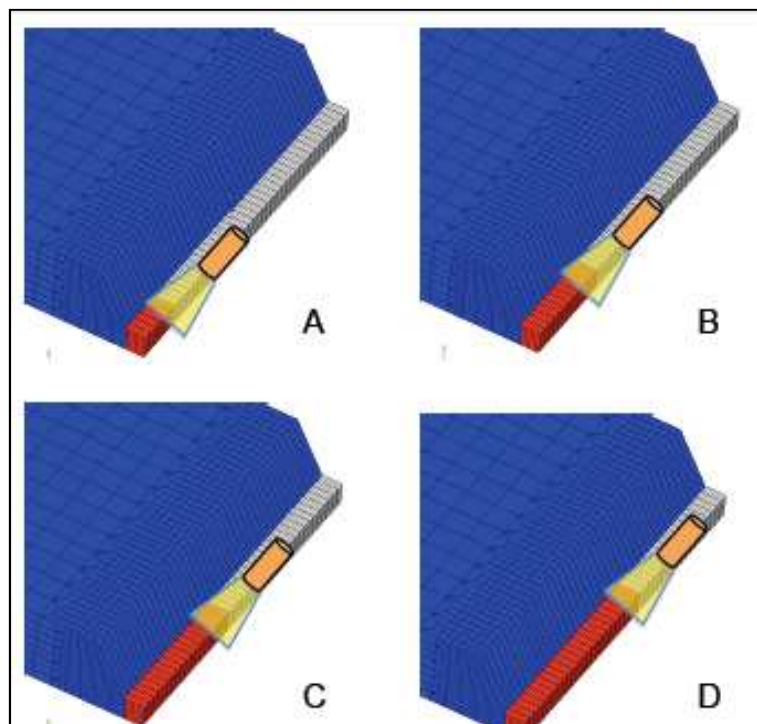

Figure 7. *Description of element birth process. The conical weld arc (yellow) moves along the weld line (A-B-C-D) in a half (symmetric) view. The inactive elements (grey) are activated after exposure to the weld arc. The birthed elements in the weld pool are indicated in red.*
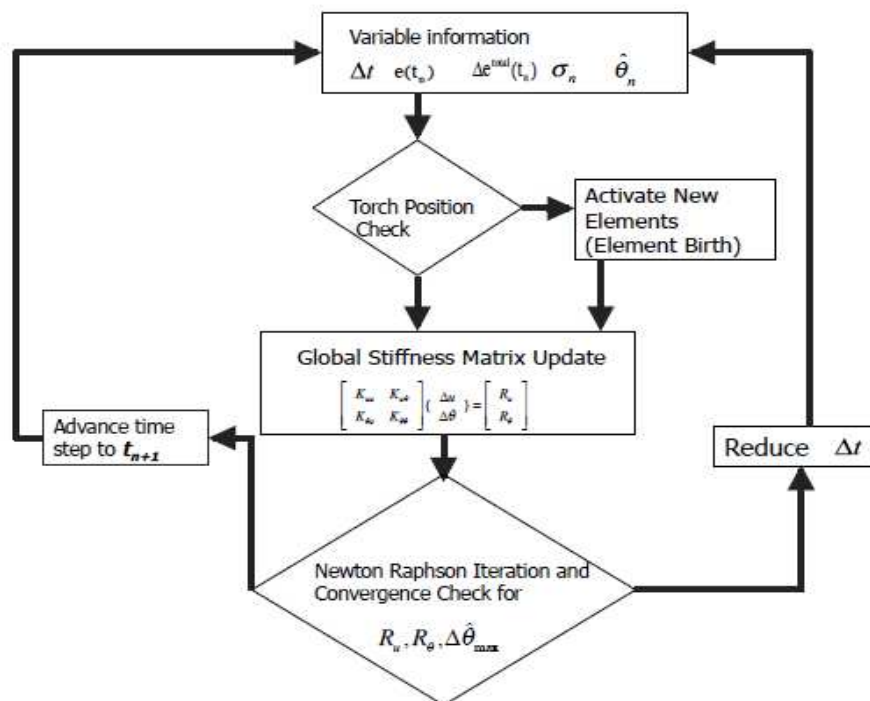
3D Multi-pass finite element welding modeling of butt-welded plate specimen
Third International Conference on Mechanical Models in Structural Engineering
University of Seville. 24-26 june 2015.

Figure 8. *Algorithmic flow chart used for each weld pass.*

2.3.2. Boundary Conditions

The two weld pieces are restrained during the welding process in a vice-like fixture. This is achieved in the finite element model (Figure 9) by restraining displacement at the top and bottom of the plate (Y direction). Also, since the momentum equation is solved without the inertial term, the displacements in all the three directions (X, Y, Z) are restrained at the face in YZ-plane at the left end. The corresponding face on the right end is free to move. This allows for expansion from the thermal changes during the welding and the cooling phase.

The thermal boundary conditions (Fig. 10) involved in this problem are two-fold. The power distribution from the weld arc to the weld-pieces and filler material is exposed to the weld-geometry as the arc moves from one end of the piece to the other. At the same time, all the surfaces of the weld geometry with nodal temperature distribution Ti, are exposed to the ambient conditions (Temperature Ta). These surfaces loose heat through convective heat transfer and radiation.
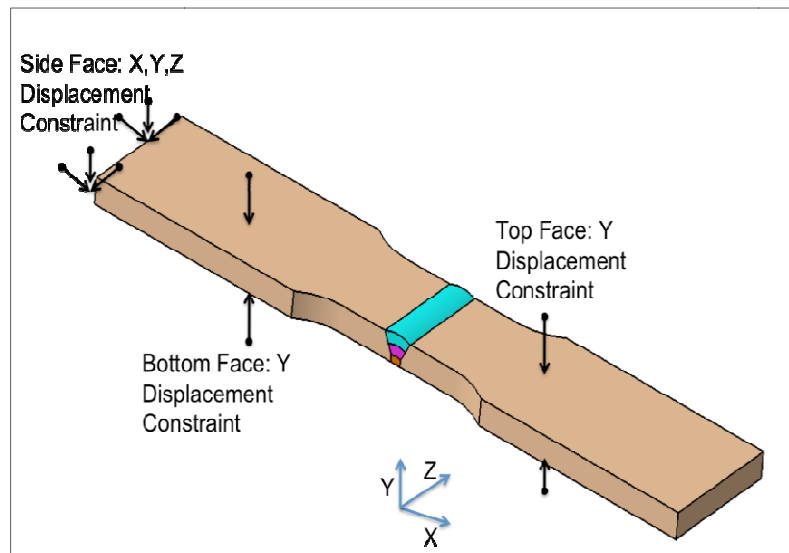
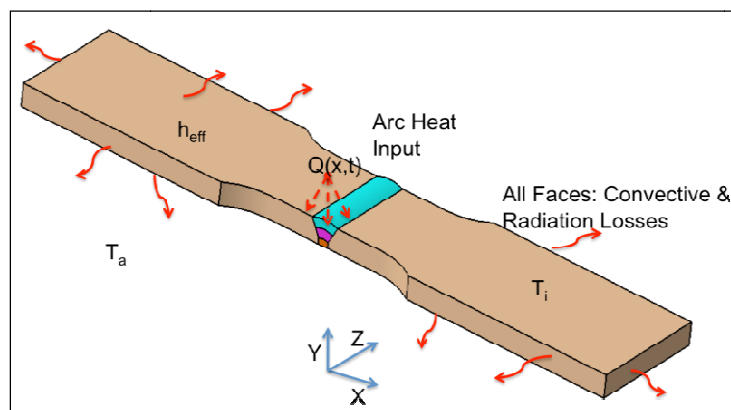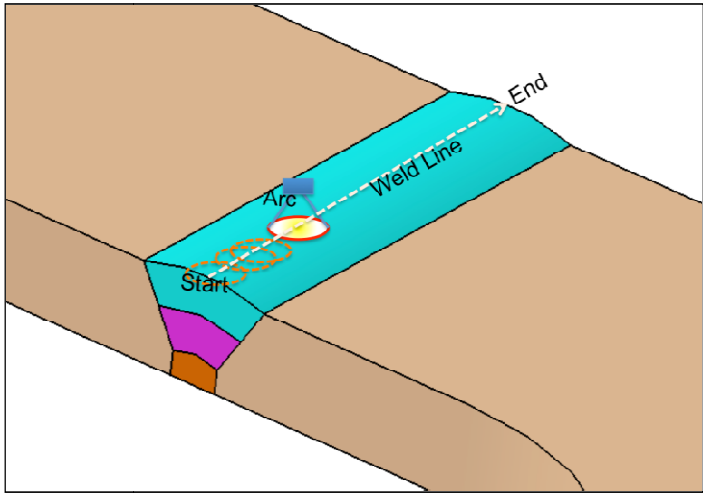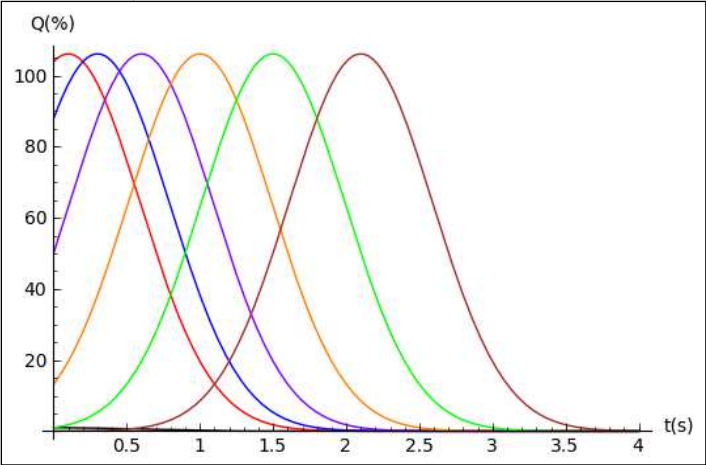**Figure 9.** *Structural boundary conditions on the weld plate.*

**Figure 10.** *Thermal boundary conditions on the weld plate.*

Figure 11 shows example distribution in space and time as the point source representing the weld arc travel along the Z axis. This weld-arc travel is implemented in the current model with the ABAQUS standard command *DFLUX with a user defined subroutine option. For all the elements of HAZ and weld pool that have a face exposed to ambient conditions, a programmed subroutine calculates resulting flux (q) at a given instant t, based on the element coordinates that are passed to the routine. At a given time instant, these calculations may be repeated several times depending on the number of iterations needed to convergence, the flux calculations may slow down the solution process significantly. In order to reduce the computations, the subroutine automatically assigns a zero value to the flux for element-faces at a distance larger than 6 mm.

3D Multi-pass finite element welding modeling of butt-welded plate specimen
Third International Conference on Mechanical Models in Structural Engineering
University of Seville. 24-26 june 2015.

(a) Arc trajectory along the weld-line

(b) Weld arc intensity distribution as the torch moves along weld line (red to brown)
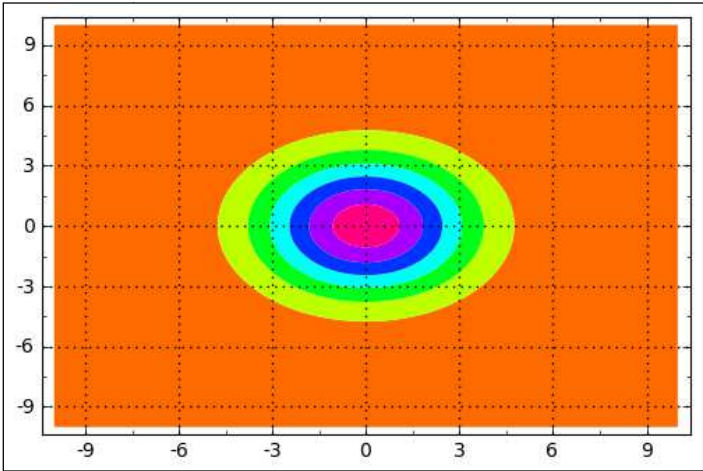
(c) Intensity distribution in the perpendicular plane

Figure 11. *Weld arc travel*

2.4. Results

The problem proposed was subjected to several computational iterations to determine feasibility of a realistic solution and within the limits of reasonable computational resources. Based on these trials, a convergent solution was obtained with the following modifications to the proposed problem:

- The element birth temperature was reduced from 2000°C to 1600°C.
- The radius of influence for surface flux from weld-arc during Pass1 was reduced from 6 mm to 4 mm to make it more reasonable.
- The efficiency of the Pass2 and Pass3 weld stages were reduced to 0.60 (60%).
- The displacement boundary condition in the thickness direction (Y coordinate) was made less restrictive by removing it for the Heat Affected Zone.
- The mechanical properties of the weld and the plate materials were described as independent of temperature while keeping the temperature dependence of the thermal properties as proposed.

To further reduce the computational demands of the problem, symmetry along the centre of the plate (symmetry in X direction) was used. The proposed symmetry reduces the displacement and thermal boundary to conditions to those shown in Figure 12 and 13 respectively. This modification allowed a finer mesh to be implemented over the problem domain while keeping the overall computational time within the limits of a desktop PC.
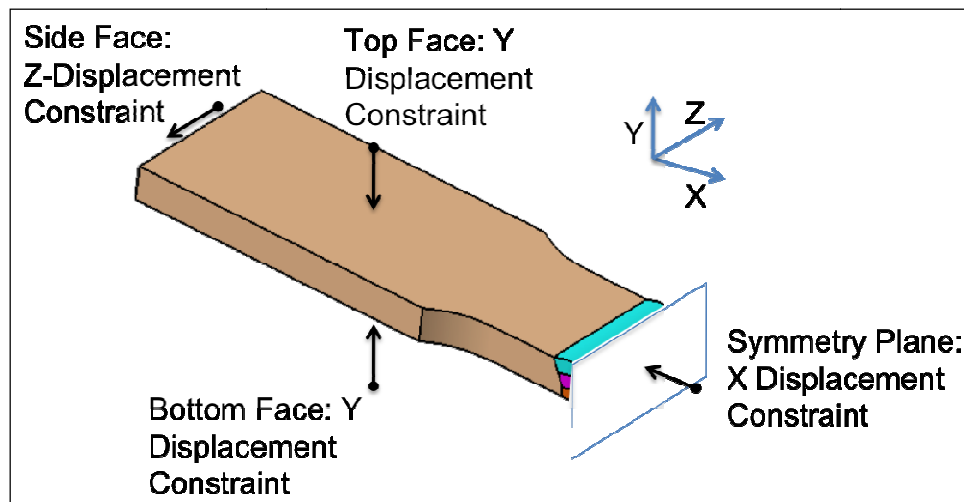

Figure 12. *Structural boundary conditions for the symmetry model*

3D Multi-pass finite element welding modeling of butt-welded plate specimen
Third International Conference on Mechanical Models in Structural Engineering
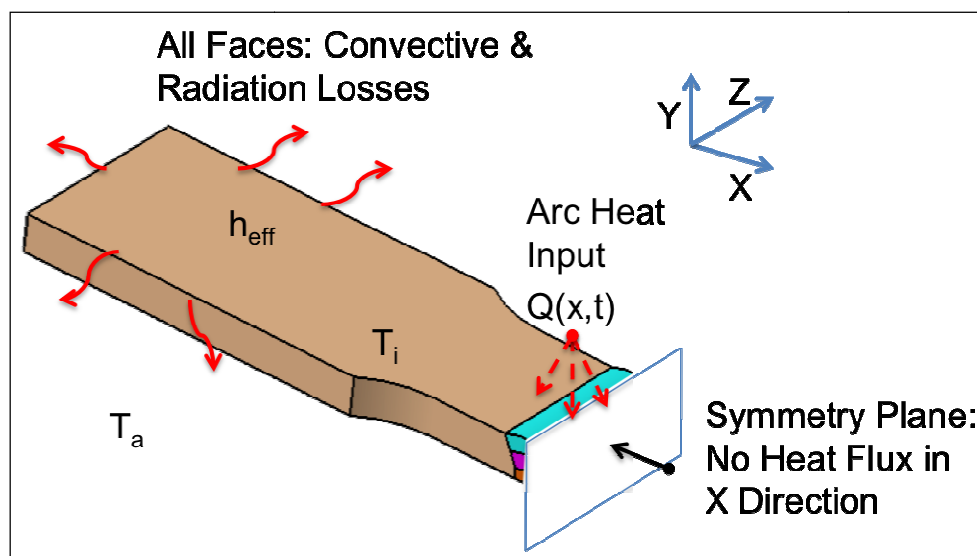University of Seville. 24-26 june 2015.

Figure 13. *Thermal boundary conditions for the symmetry model*

Table 3 shows the mesh details for the half-symmetry model. As expected, the simulation of the weld-passes is computationally far more challenging than the simulation of the cooling stages at the end of each weld-pass. Yet, the time required for minimum cooling is variable based on the criteria that the maximum temperature in the specimen must be less than 250°C. Based on the speed of welding for each pass and the cooling period based on this criterion, the physical time simulated in the final problem is shown in Table 4. A graphical representation of the welding operation sequence in terms of total heat input to the system is shown in Figure 14.

Table 3. Mesh details for the half-symmetry model

Element Sets	No. of Elements	No. of Nodes
Model	19628	20885
Pass1	2100	2982
Pass2	2940	3976
Pass3	2520	3479

Table 4. Final data for length of physical time for individual welding stages

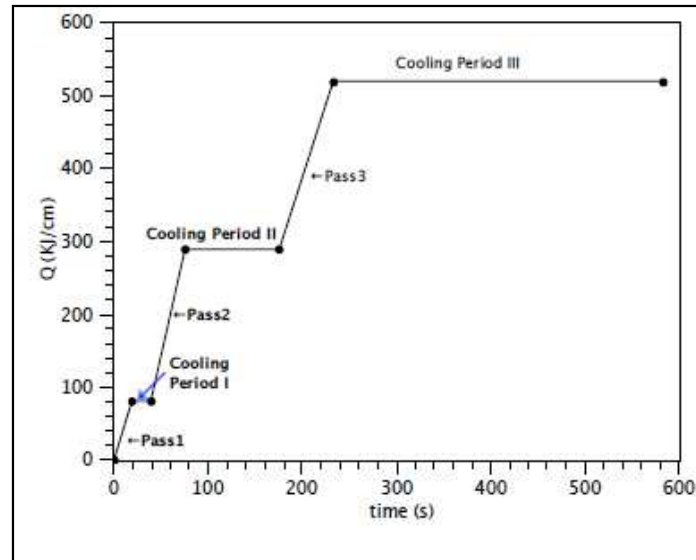| Weld Pass	Torch Travel Time(secs)	Cooling Time(secs)
Pass1	19.25	20
Pass2	36.2	100
Pass3	57.4	350

Figure 14. *Sequence of simulated operations in terms of chronological heat input.*

2.4.1. Weld-Pass Simulation Data

Graphical results show the time evolution of the key thermal variables in the simulation –temperature and heat flux- for the successful simulation trial. As the weld-torch moves in the transverse (Z) direction, successive elements of the weld-pool are birthed approximating deposition of the weld-material in the liquid state. The deposited weld-material is also being heated by the surface flux from the weld-arc. The weld-arc also heats the part of the specimen plate in the HAZ region. This heating of the plate edge (HAZ) and the deposited weld-material is in the narrow time-frame when the distance of the weld-arc is within the radius of influence for the arc. As the distance between a particular point in the HAZ and the weld-pool region increases beyond the effective radius of influence, the particular point starts losing heat through radiation and convection. A successful weld is formed only if fusion between the HAZ and the weld-pool takes place. The thermo-mechanical history of select nodes chosen as marker points illustrates the transients experienced by a given node in the model. Figure 15 shows a few marker points in the YZ-plane cross-section through the centre-line in the longitudinal (X) direction. Points {a1, b1, c1} lie on the weld-line for Pass1, 2 and 3 respectively. Similarly points {a2, b2, c2} lie along the fusion lines for the 3 passes and points {a3, b3, c3} are the corresponding points on the boundary of the HAZ and the plate. Points {a4, b4, c4} are chosen at, approximately, 4mm from the heat affected zone and are chosen to represent the far-field behaviour. Figure 15 also shows the temperature history of these nodal markers for the respective weld-passes. As expected, the markers along the weld-lines show highest temperatures. The temperature of these nodes starts at 1600°C corresponding to the birthing temperature. This is followed by increase in the temperature as the weld-arc heats the deposited material. As the distance of the weld-arc from these nodes increases beyond the radius of influence (4 mm for first pass and 6 mm for 2nd and 3rd pass), the temperature of these nodes continuously falls down. For a node further away from the symmetry plane or the weld-line, there is a similar increase and decrease of the temperature with the motion of the weld-arc. For a node at the beyond the fusion line, there is almost no heating from the surface-flux. So for

3D Multi-pass finite element welding modeling of butt-welded plate specimen
Third International Conference on Mechanical Models in Structural Engineering
University of Seville. 24-26 june 2015.

much of the HAZ and the rest of the plate, the temperature rise is purely from heat conduction from the weld-pool.

During the heating from the weld-arc the weld-pool and the parts of the HAZ expand creating compressive stressing along the fusion boundary (fusion plane). With the solidification and the cooling of the deposited-weld material, there is continuing contraction of the weld-pool region. This relieves some of the compressive stresses and may even result in tensile stresses. Since the heating and cooling of the weld-pool and the HAZ region is in a chronological fashion rather than simultaneously, it creates additional stress gradients in the weld direction (Z).
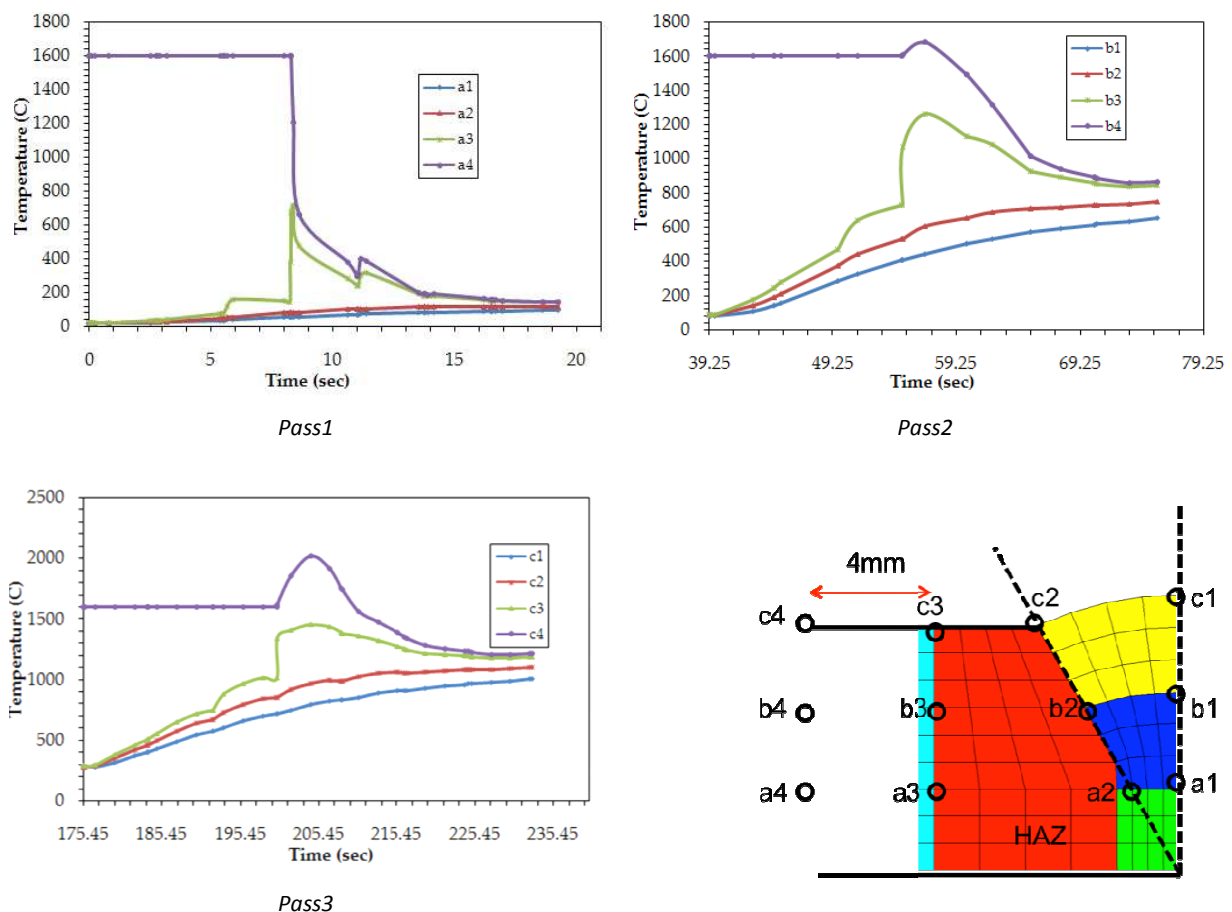

Pass1

Pass2

Pass3

Figure 15. *Temperature history for select marker points during weld pass.*

2.4.2. Weld Cooling Simulation Data

From the thermo-mechanical origin of stresses in the welded plates, it is clear that the temperature is the primary driver of the stress evolution in the welding process. More often than not, the first weld-pass in a multi-pass weld-joint is initiated with the two plates completely at room temperature. Yet, for practical reasons associated with the cost of welding operation, it is not always possible to initiate the subsequent passes with the plates and the joint at uniform or room temperature. While, higher

initial temperature is advantageous from the point that the fusion between HAZ and the weld-pool is helped by higher temperature, the fact that this temperature distribution is highly non-uniform introducing associated (non-uniform) residual stresses. For these reasons, the part cooling after each pass is an important practical step.

In the present simulations, the welded plates are cooled for a period long enough to achieve temperature no more than 250°C in the welded plates. The data for the cooling stages is presented in a sequence identical to the previous section. Figure 16 shows the time history of select nodal markers. The temperature variation for all the nodal markers is monotonically decreasing, which is characteristic of the cooling law for a body cooling from an initial high temperature. The overall distribution of temperatures in the region of interest is shown as a contour plot at the end of each of the cooling stage.
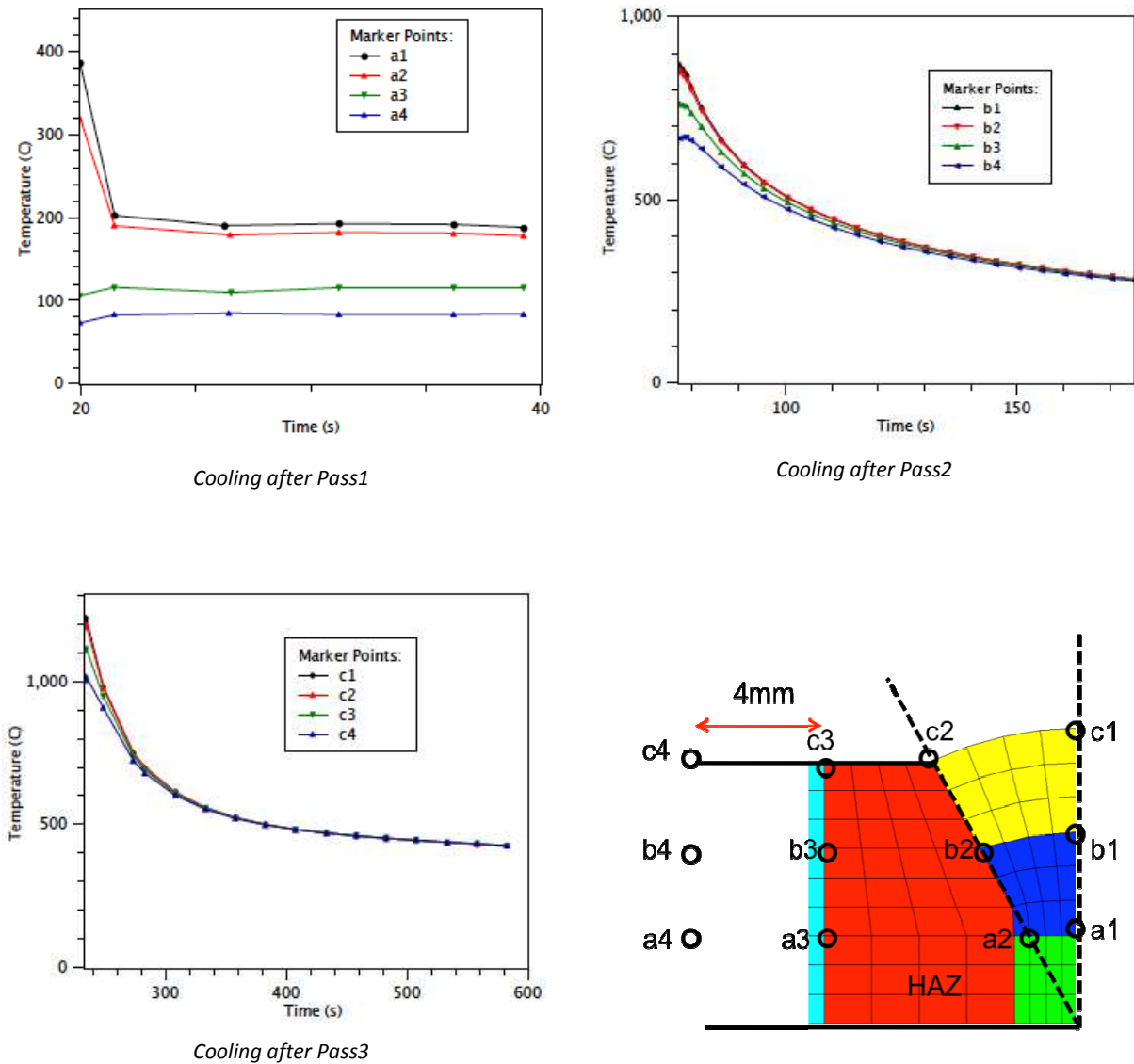

Cooling after Pass1

Cooling after Pass2

Cooling after Pass3

Figure 16. *Temperature history for select marker points during cooling stages*

3D Multi-pass finite element welding modeling of butt-welded plate specimen
Third International Conference on Mechanical Models in Structural Engineering
University of Seville. 24-26 june 2015.

The stress contours at the end of individual weld passes discussed in previous section, undergo a thermo-mechanical relaxation process with the decreasing temperatures as part of the cooling process. The stress contours at the end of the cooling stages show this relaxation of stresses through overall lower level of stresses. Since the volume of the material deposited in each weld pass is substantially different, the length of cooling period for each of the cooling stage is proportionately longer for successive cooling stages. Figure 16 also shows variation of temperature along critical geometrical paths. When compared to similar plots at the end of weld-passes, the variation of the temperature along centre-line, weld-line and fusion line all indicate a far more uniform spatial distribution of temperatures. Although the level of stresses is reduced, the part still shows significant level of residual stresses from the welding process. Also, in case of successive passes, the residual stresses are also contributed by the level of cooling (mainly through time-duration) and heating (during weld passes). It is important to note that even after nearly seven minutes of cooling period after the third weld-pass, the fusion line shows significantly large Von-Mises stresses (Fig. 17). The following section discusses the implications of these results in detail.
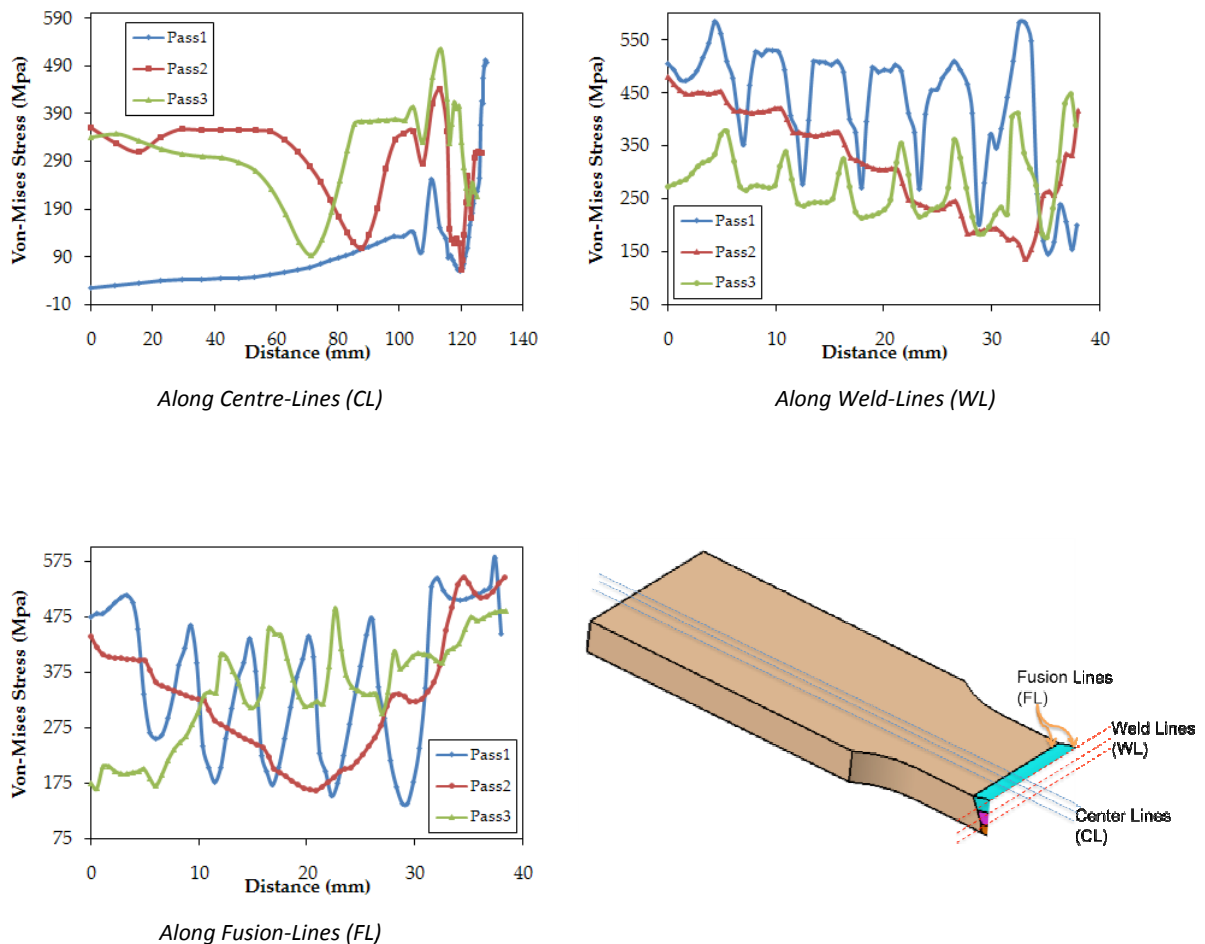

Along Centre-Lines (CL)

Along Weld-Lines (WL)

Along Fusion-Lines (FL)

Figure 17. *Von-Mises stresses at the end of cooling stage along selected paths*

3. CONCLUSIONS

The proposed multi-pass weld problem was modified before a reasonable solution could be obtained. This circumstance was needed because of heavy distortion of the elements in successive passes.

3.1. Justification to Problem Modification

After several trial runs and careful elimination procedure, the heavy distortion of the elements was linked to excessive heat input. Typically, the molten weld material is deposited in the form of a liquid-drop. The variation of the temperature of this drop is typically around 200-300°C above the liquidus temperature. Assuming a linear variation of the temperature from the centre of a spherical drop to the outside, the average temperature of the drop reached around 1600°C. This formed the basis of a decrease in the temperature of the birthing elements by 400°C (from 2000°C to 1600°C) in the final simulation.

Additionally, the torch-radius was reduced to 4 mm for pass1. This assumption was reasoned through practical aspects of the welding procedure. The half-width of the pass1 weld-pool is only around 2-3 mm. Thus a torch-radius of 4mm is suitable to heat the relevant HAZ and weld pool without dispersing the heat over a much larger area.

Lastly, the power input for weld-pass2 and pass3 were reduced by 75% of the initially proposed power input for those passes. These ones involve a larger amount of material deposition and use GMAW welding process. This is achieved by increased power input as well as a longer exposure of the weld arc during the weld-pass. The additional exposure is achieved by weaving the torch along the weld line. This additional motion in the longitudinal direction is necessary in practice so that the extreme edges of weld-pool receive adequate heat during the arc travel. In the current simulation, the weaving motion of the weld-torch is not simulated. Yet, the weld-torch speed is reduced proportionately to account for the increased exposure time. This has an undesired effect in excessive heating closer to the symmetry-plane along the weld line. The nature of heat-distortion during the previous unsuccessful trial runs indicated excessive localized heating as the probable source. Further trials with a 75% lower power proved adequate in controlling the mesh distortion.

3.2. Concluding Remarks

The overall variation of the stresses in the plate show similar trends to those described in literature [2, 4, 5, 6, 7, 8]. The weld plate dimension is smallest in the Y direction. This means that part will cool faster in the through-thickness direction. As a result, the Y component of the normal stresses is the smallest, followed by the transverse Z components. Because of the constraints arising from the symmetry conditions as well as the end boundary conditions, the longitudinal (X) normal stress component is the largest stress. As the weld-arc travels from one end to another end in the Z direction, it creates an asymmetric stress distribution from one end to another (compressive to tensile). Similar non-symmetry is seen in the longitudinal as well as through-thickness direction. The stress results in this study do show high fluctuations in both time-history plots as well as the spatial

3D Multi-pass finite element welding modeling of butt-welded plate specimen
Third International Conference on Mechanical Models in Structural Engineering
University of Seville. 24-26 june 2015.

distribution plots along weld line, centre line and fusion lines. While these fluctuations are present in all three weld-passes, their effect is far more pronounced in pass1 and pass3. Closer observation indicates that the frequency of these fluctuations is related to the element birth frequency. While, these fluctuations may represent physical solution, a finer discretization for smaller, more numerous element-birth steps could lead to a smoother solution. On the contrary, it is possible that for the weld pass2 the element birth-rate matches the weld material deposition speed accurately. This proves the utility of the computer simulation in obtaining a smooth (low stress) weld joint as changing the element birth rate in the simulations could be used as an instrument to determine a low-residual stress joint. The element birth-rate is determined ad-hoc based on the duration of the weld pass (weld speed and the length of the weld) and the level of element discretization in the direction of the weld. Table 5 shows a few select trials where element birth strategy was varied in order to obtain a convergent solution. During the simulation, the element birth is essentially implemented as a "discontinuous step". The introduction of the newly born elements at high temperature requires a thermo-mechanical step to equalize the temperature and stress variables. In the event of an element birth rate that is far from a "physical" weld deposition rate, the instability from this discontinuous step can lead to fluctuations in the solutions or in the worst case scenario, numerical instability. Figure 18 shows the time history of temperature and maximum principal stress at the nodal markers discussed in the previous section. The discontinuities in the variables due to element birthing process are marked by arrows in the figure. Despite the instantaneous sharp "glitches" both the temperature and maximum principle stresses show quick recovery and a continuous "envelope" for the variable solution. This firmly establishes the validity of the current solution with the proposed element birth rates to a degree. Yet, the effect of the chosen element birth rate on the fluctuations in spatial distribution of stresses may or may not be realistic. Actual experimentation to obtain physically valid weld conditions would prove valuable in such a case.

Additionally, the shape of the weld pool was chosen in an ad-hoc manner with the relative volume ratios as the constraint. This may have a large effect on the quality of simulation for a physically stable solution. If the chosen shape is not a thermo-mechanically stable shape for the range of temperatures corresponding to the liquidus temperature on one end and solidified shape after cooling, instabilities will occur in the simulation. A more rigorous approach guaranteeing a stable solution will start with a weld-pool shape derived from an analytical solution [3]. Given these observations, it is quite possible that the relatively stable solution of weld pass2 was achieved by the accuracy of the weld pass geometry for the given deposition rate simulated by the element birthing procedure for the particular pass.

Nevertheless, the final solution shows crucial stress distributions in a challenging geometry where large thermal transients and gradients are created by the welding procedure. The results also indicate the plastic yielding of the weld-joint after extensive cooling of the joined plate. The displacements from the results can be used to estimate the extent of distortions qualitatively. Despite minimal resources (2 CPUs on a standard Intel desktop architecture and 2 GB RAM over duration of 4 days) the procedure is able to provide adequate details in predicting residual stresses for multi-pass welded components. It is recommended that tools developed in this study, are applied to a more practical problem.
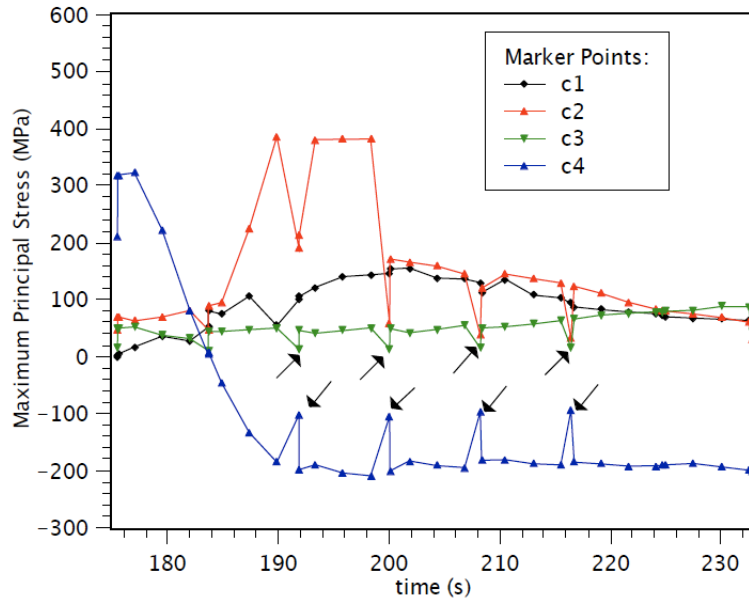
Maximum principal stress
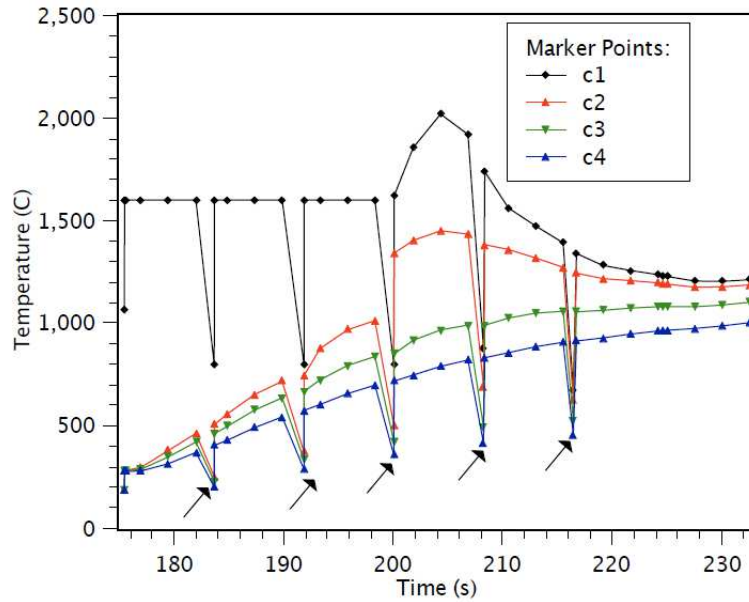
Temperature

Figure 18. *Time history of nodal markers for maximum principal stress and temperature during Pass3. Arrows indicate occurrence of element birth.*

3D Multi-pass finite element welding modeling of butt-welded plate specimen
Third International Conference on Mechanical Models in Structural Engineering
University of Seville. 24-26 june 2015.

Table 5. Select trials for element birthing rate

Specimen (thickness)	Elements along Weld-line	Element Set	Steps per Weld Stage	Failure (y/n) (Step)	Weld Travel	Time of Failure (Weld Pass)
8 mm	42	Slice_225	14+1(cooling)	Y (Pass2)	21.9mm	60.1 (Pass2)
8 mm	70	Slice_231	14+1(cooling)	Y (Pass2)	16.4mm	49.6 (Pass2)
8 mm	70_slices_temp_independent (birth_rate_20_slices/step)	Slice_241	8+1(cooling)	Y (Pass2)	21.7mm	60.1 (Pass2)
8 mm	70_slices_temp_independent	Slice_220	14+1(cooling)	Y (Pass2)	17.2mm	54.9 (Pass2)
20 mm	14_slices_temp_independent		21(no cooling)	N	NA	NA

REFERENCES

[1] Sanz Balduz, L.J. (2012). *2D Multi-Pass Finite Element Welding Modelling of Butt-Welded Plate Specimen* (PhD. thesis). Santander: Universidad de Cantabria.

[2] Fanous, I.F.Z. (2002). *3D Modeling of the Welding Process Using Finite Elements* (M.Sc. thesis). El Cairo: American University in Cairo.

[3] Nguyen, N.T., Ohta, A., Matsuoka, K., Suzuki, N. & Maeda, Y. (1999). Analytical Solutions for Transient Temperature of Semi-Infinite Body Subjected to 3-D Moving Heat Sources. *Welding Journal Supplement, August 1999, 265-274.*

[4] Zakaria, T., Vitek, J.M., Goldak, J.A., Debroy, T.A., Rappaz, M. & Bhadeshia, H.K.D.H. (1995). Modeling of Fundamental Phenomena. *Modelling and Simulation in Material Science and Engineering, 1995-3, 265*.

[5] Dong, P. (2001). Residual Stress Analyses Multi-Pass Birth Weld: 3-D Special versus Axisymmetric Models. *ASME Journal of Pressure Vessel Technology, 123, 207-213.*

[6] Friedman, E. (1975). Thermomechanical Analysis of the Welding Process Using the Finite Element System. *ASME Journal of Pressure Vessel Technology, 97, 206-213.*

[7] Zakaria, T., Vitek, J.M., Goldak, J.A., Debroy, T.A., Rappaz, M. & Bhadeshia, H.K.D.H. (1995). Modeling of Fundamental Phenomena. *Modelling and Simulation in Material Science and Engineering, 1995-3, 265.*

[8] Wilkening, W.W. & Snow, J.L. (1993). Analysis of Welding-Induced Residual Stresses with the Adina System. *Computers and Structures, 47-1993, 767-786.*